Polymer Degradation and Stability 155 (2018) 35–42

Contents lists available at ScienceDirect

Polymer Degradation and Stability

journal homepage: www.elsevier.com/locate/polydegstab

Effect of hydrolytic degradation on the mechanical property of a thermoplastic polyether ester elastomer

Cody M. Diaz [a], Xiang Gao [b], Agathe Robisson [c, 2], Miranda Amarante [c], S. Sherry Zhu [c, *, 1]

[a] Department of Chemical Engineering, Massachusetts Institute of Technology, 77 Massachusetts Ave., Cambridge, MA, 02139, USA
[b] Department of Chemistry, Rutgers University, Piscataway, NJ, 08854, USA
[c] Schlumberger-Doll Research, 1 Hampshire Street, Cambridge, MA, 02139, USA

ARTICLE INFO

Article history:
Received 2 November 2017
Received in revised form
1 June 2018
Accepted 5 July 2018
Available online 6 July 2018

Keywords:
Thermoplastic elastomers
Hydrolytic degradation
Chemicrystallization
Kinetics
Morphology
Mechanical properties

ABSTRACT

Polymers with a finite lifetime are of great interest for oil and gas industry. Thermoplastic elastomers (TPEs) combine the strength of thermoplastics with the flexibility of elastomers, a characteristic also potentially useful in oil and gas applications. We studied the hydrolytic degradation of a TPE of interest at elevated temperatures from both a mechanical and chemical perspective, and have demonstrated that the chemical degradation rates, the change in crystallinity and the storage modulus all follow the pseudo zero order kinetics with respect to varying time at three temperatures. Applying Arrhenius' empirical relationship to the determined rates gives rise to a temperature-dependent model that predicts the degradation behavior of the TPE outside of the experimental temperature range. Our results indicate that hydrolytic degradation leads to an increase of crystallinity (chemicrystallization) and a decrease of tensile strength and strain, and that the increase of crystallinity strongly correlates to the increase of the storage modulus. The polymer eventually deteriorates due to brittleness.

1. Introduction

Polymers with a finite lifetime are of great interest for the medical device, electronics [1,2], and oil and gas industries [3]. A controlled degradation of the materials within a defined time frame could enable transient applications that increase operational efficiency and reduce the overall cost of producing oil and gas. Degradable materials are highly desired for some transient applications in hard-to-reach locations of the downhole environment [3,4]. The degradable materials will dissolve into downhole fluids or lose their integrity by degrading to small particles or powders upon passive or active triggers after fulfilling their temporary functions as a device or a seal. Although all polymers eventually fail due to wear, tear, or aging, polymers with controlled degradation, which predictably degrade with property changes as a function of time, are critical for these potential applications.

We are particularly interested in degradable elastomeric materials that can be used as temporary seals and plugs. Conventional elastomers, such as hydrogenated nitrile butadiene rubber (HNBR), ethylene propylene diene monomer rubber (EPDM) etc., have lifetimes longer than the requirement of transient applications for downhole use. Thermoplastic elastomers (TPEs), on the other hand, may contain hydrolysable functional groups [5] such as esters, urethanes, and amides that experience hydrothermal degradation in downhole conditions. TPEs have networks formed by physical crosslinking that could be physically or thermally reversible, thus they combine the strength of plastics with the flexibility of elastomers. TPE have been used in a variety of applications including wire insulation, automobile fascia, footwear, wheels and adhesives. [6]· [7] Most of the TPEs are used in an ambient condition, and thus are perceived as tough and durable materials. However, several conditions in the downhole environment affect TPE properties: rising temperatures and water penetration into the materials soften the TPEs, while hydrolytic degradation of the polymer chains may result in a change of morphology and mechanical properties of the materials. Our goal is to understand the property change of the TPE when it undergoes hydrolytic degradation in downhole conditions, so that we can design components whose property evolutions are fully understood and predictable during their lifetime downhole. This paper reports our studies of the kinetics and evolution of properties of a

* Corresponding author.
E-mail address: Shitong.zhu@aramcoservices.com (S.S. Zhu).
[1] Present address: Aramco Services Company Boston Research Center, 400 technology Square, Cambridge, MA 02139, USA.
[2] Falculty of Civil Engineering, Vienna University of Technology, A-1040, Vienna, Austria.

https://doi.org/10.1016/j.polymdegradstab.2018.07.002
0141-3910/

particular TPE, polyether ester, poly-(butylene terephthalate)-co-(tetramethylene ether) glycol terephthalate (PBT-PTMG), when undergoing hydrothermal degradation.

2. Experimental

2.1. Materials

The PBT-PTMG was sourced from E. I. du Pont de Nemours and Company (DuPont Hytrel®). The polymer samples are flat sheets with a thickness of 1.5–3 mm. The glass transition temperature (T_g) of the PBT-PTMG is 25 °C, and the melting point (T_m) is 218 °C. Fig. 1 shows a generic structure of the PBT-PTMG.

Benzyl alcohol and 0.0204 N KOH in methanol were purchased from Sigma Aldrich. Phenolphthalein indicator (0.5% (w/v) in 50% (v/v) in methanol was purchased from Ricca Chemical Company.

2.2. Hydrolytic degradation

For most experiments, rectangular beam-shaped samples (22 × 4x3 mm) were die cut randomly from large sheets and subjected to an experimental degradation procedure. The mass, volume, dimensions, and storage modulus of each original sample were measured. Then, three samples were sealed in glass vials with approximately 10 ml of DI water and placed in an oven at 98 °C for varying time intervals. After desired time, the samples were cooled to room temperature and taken out of the water, their surface was wiped using Kimwipes. Their mass, volume, dimensions, and storage modulus at room temperature were measured again. Next, the samples were dried at room temperature under vacuum until the measured weight was constant (about 1 week). The mass, volume, dimensions, and storage modulus (temperature sweep) of the dried samples were then measured. For degradation experiments conducted at higher temperatures, the samples in un-sealed vials were placed inside a pressure vessel (Figure S1c, supplementary materials), and the pressure vessel was sealed and placed in an oven at either 120 °C or 150 °C for varying time intervals.

For tensile strength measurements, dog bone-shaped specimens (ASTM D638-type V) having roughly a thickness of 1.5 mm were stamped using a die from the same sheets as above. Samples were placed in a 100 ml Schott vial full of DI water (3 samples per vial), then placed in a pressure vessel with extra water for different amounts of time (7 h, 14 h, 1 day, 1.2 days, 2 days, 2.6 days, 3 days, and 4 days) at 120 °C. The tests at 14 h and 2.6 days, which correspond to transitions, as described below, were repeated. At each time interval, six samples were taken out. Three samples were tested right away in the wet state, at room temperature, and three were left to dry in a vacuum oven at room temperature for at least a week before testing at room temperature. The reference sample ("Ref") was only dried in the vacuum oven.

2.3. End group analysis

The hydrolysis of PBT-PTMG results in an increase of the acid end groups. The rate of hydrolysis of the PBT-PTMG in water can therefore be tracked by titrating the quantity of acid end groups in the original and the degraded samples. The dried polymer sample with known weight (around 0.3 g) was dissolved in 10.0 ml of benzyl alcohol after heating at 170 °C under N_2 for 30 min. Around 8 drops of phenolphthalein indicator were added into the clear solution. The concentration of the acid end groups in each sample was titrated at 170 °C under N_2, using 0.0204 N KOH (N_{KOH}) in methanol, and the end point was determined when the color of the solution turned to light pink. The blank titration was carried out using 10.0 ml of benzyl alcohol at 170 °C under N_2. The concentration of the end group (mol/g) was calculated using Equation (1):

$$[RCOOH] = \frac{(V_p - V_b)*N_{KOH}}{1000*W_p} \quad (1)$$

V_p is the volume (ml) of KOH solution for titrating the polymer and V_b is the volume (ml) of KOH solution for titrating the blank. W_p is the mass of the polymer sample.

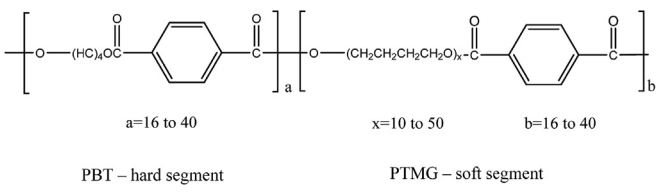

Fig. 1. A generic structure of the PBT-PTMG thermoplastic elastomer.

2.4. Differential scanning calorimetry (DSC)

We measure the melting and crystallization temperatures and enthalpy of the PBT-PTMG samples before and after degradation using differential scanning calorimetry (TA Instruments, Q200). Around 10 mg of the polymer samples were sealed in an aluminum pan and loaded to the auto-sampler of the DSC. The samples were equilibrated at −50 °C, ramped to 250 °C at 10 °C/min, and then cooled back down to −50 °C at 10 °C/min. The scan was repeated once. The specific enthalpy of melting was determined by integrating the peak of melting from the first scan. The percentage of crystallinity (X_c) was calculated according to Equation (2) using the specific melting enthalpy of PBT ($\Delta H_m^{PBT,crystal} = 145.3$ J/g) [8].

$$Xc\% = \frac{\Delta H_m^{TPE}}{\Delta H_m^{PBT,\ crystal}}\ x\ 100\% \quad (2)$$

2.5. Dynamic Mechanical Analysis (DMA)

We determined the storage modulus of the samples using Dynamic Mechanical Analysis (TA Instruments Q800). A 0.1% strain amplitude was applied at a frequency of 1 Hz. The temperature was ramped at 5 °C/min to 160 °C after equilibrating at 28 °C. The storage (elastic) modulus E' at 100 °C was recorded for each sample before and after degradation.

2.6. Transmission electron microscopy (TEM)

An electron micrograph on a thin slice of elastomer was obtained using a TEM (JOEL 2100, courtesy of the Center for Nanoscale Systems at Harvard University). The accelerating voltage (high tension, HT) of the TEM was set at 80 kV and the filament was set to 60%. The elastomer sample was sectioned to a thin slice (less than 20 nm in thickness) using an ultramicrotome at room temperature. The sample was trimmed into smaller blocks using a metal blade first, and then cooling with liquid N_2 before sectioning into thinner slices using a diamond blade equipped with a water bath. The slices were picked up from the water using a copper grid. The grid with the sample was immersed in a 0.2% aqueous solution of phosphotungstic acid (PTA) for 15 min and then washed and air dried. The amorphous phase absorbs the stain and the crystalline phase is then visible as a light/bright fibrillary region under TEM [9].

2.7. Tensile testing

A 5565 series Instron machine equipped with a 5 kN load cell was used to measure the tensile strength of the samples. The tests were done at a crosshead displacement rate of 500 mm/min. The strain was calculated by dividing the crosshead displacement by the gauge length of the sample (the gauge length was estimated to be 23 mm). The stress was calculated by dividing the load by the initial cross-section of the sample.

3. Theory and calculation

3.1. The apparent rate constant of hydrolysis

Chemical degradation of PBT-PTMG is the result of hydrolysis of the ester bonds in the polymer chains to form a carboxylic acid and an alcohol end group. Water diffusion and hydrolysis occur predominately in the amorphous phase [10], similar to other hydrolytic degradable semicrystalline polymers [11]. Since the samples are immersed in water during the experiments and water diffusion is not the rate limiting step as demonstrated later for these thin experimental samples, the reverse condensation reactions are considered minimum. The reaction follows a pseudo zero order reaction mechanism (Equation (3)) wherein the concentrations of water ($[H_2O]$) and the ester bonds $[RCOOR']$ inside the sample can be considered as constant, and assuming the contribution of acid end groups $[RCOOH]$ catalyzed hydrolysis is minimum at the early stage of hydrolysis [12]. The number average molecular weight M_n is inversely proportional to the concentration of acid end group.

$$
\begin{aligned}
&-\frac{d\left[RCOOR'\right]}{dt} = \frac{d[RCOOH]}{dt} = k\left[RCOOR'\right][H_2O] \\
&\frac{d[RCOOH]}{dt} = k', \quad k' = k\left[RCOOR'\right][H_2O] \\
&[RCOOH]_t = k't + [RCOOH]_0 \\
&\frac{1}{M_{nt}} = k't + \frac{1}{M_{n0}}
\end{aligned}
\tag{3}
$$

The slope of the plot of $[RCOOH]_t$ vs time t is the apparent rate constant k' at the given temperature. M_{n0} and M_{nt} are the number average molecular weight of PBT-PTMG at time 0 and time t, respectively. We can define $t_{1/2}$ as the time when M_n decreases by 50%. So $t_{1/2} = 1/M_{n0}k'$.

4. Results and discussions

4.1. The kinetics of hydrolysis

To demonstrate that water diffusion is not the rate limiting step and that there is uniform hydrolysis through the entire sample, we first measured the rate of water diffusion at the experimental temperatures for hydrothermal degradation. The detailed experimental procedure and theoretical details for measuring and calculating water diffusion coefficient D_x are in the Appendix. Table 1 shows the measured D_x for the PBT-PTMG at three experimental temperatures. The temperature-dependence of D_x follows the Arrhenius equation (Appendix). The experimentally measured activation energy E_a for D_x is 35.2 kJ/mol. Since the diffusion coefficients at temperatures higher than 100 °C are difficult to measure accurately, we used Arrhenius' equation to predict D_x at temperatures up to 150 °C. Table 1 presents the predicted D_x at 120 °C and 150 °C. The conservative estimations of the time taken to saturate a 3 mm thick sample from one-dimensional water diffusion ($t_s = \left(\frac{a}{4}\right)^2 \frac{\pi}{D_x}$, t_s is time to water saturation) are 6.1, 3.20 and 1.49 hrs at 98, 120 and 150 °C, respectively. In fact, the experiments also confirm that the water concentrations remain constant at even significantly longer degradation time than t_s,: $1.00 \pm 0.3\%$ for one month at 98 °C, $1.12 \pm 0.04\%$ for 86 h at 120 °C, and $1.46 \pm 0.09\%$ for 18 h at 150 °C (Figure S2 in Supplementary Materials).

Because the products (oligomers) from the PBT-PTMG hydrolysis have low solubility in water, the samples have little mass loss (<0.2% weight loss) throughout the entire degradation time at each temperature (Figure S2 in Supplementary Materials). Thus, tracking the mass change of the sample following the hydrothermal degradation is not feasible to study the degradation kinetics. We attempted to track hydrolysis using ATR-FTIR to monitor the concentration of ester or acid end groups. However, due to the low concentration of the acid end groups even after hydrolysis and the overlapping of the carbonyl peaks of acid ($1674\ cm^{-1}$) with that of the ester ($1714\ cm^{-1}$) groups [13,14], an accurate integration of the two peaks could not be obtained (Figure S3 and S4, Supplementary Materials). Notable changes in the FTIR spectrum after degradation appear as increases of the peak intensities at $917\ cm^{-1}$ and $751\ cm^{-1}$, contributed by the motions of -$(CH_2)_4$-O- in the polymer chains in both hard and soft segments. The result suggests changes of crystallinity and possible conformation after degradation (Figure S3, Supplementary Materials) [14].

Titration of the acid end groups [15] (end group titration) on the original and the degraded sample provided a more robust method of tracking the kinetics of hydrolysis. The number average molecular weight decreases as the degradation proceeds at each temperature (Figure S5, Supplementary Materials). As shown in Fig. 2, $[RCOOH]_t$ vs degradation time follows the pseudo zero order reaction kinetics at each degradation temperature as illustrated by Eq. (3). The apparent rate constants of hydrolysis are 3.53E-11, 1.37E-10 and 9.92E-10 s^{-1} at 98, 120 and 150 °C respectively (Table 1). The corresponding activation energy E_a for the hydrolysis is 84.0 kJ/mol (Figure S6, Supplementary Materials). Using E_a for the hydrolysis reaction, we are able to calculate the rate constant of hydrolysis at 38 °C and 70 °C (Table 2). To illustrate the impact of temperature on the rate of material degradation, we present $t_{1/2}$ (the time taken to degrade 50% of the ester bonds i.e. reduce M_n by 50%) in Table 1, which indicates that 50% of the ester bonds will be hydrolyzed within two weeks at temperatures above 98 °C.

Table 1
Diffusion coefficient of water into TPE.

Temperature (°C)	D_x (m^2/s)	Predicted D_x (m^2/s)	t_s for 3 mm thick sample (hrs)	Hydrolysis rate constant k' (s^{-1})	$t_{1/2}$ (days)
38	9.84E-12[m]	9.28E-12[c]	54.7	1.72E-13[c]	1544.0
70	2.87E-11[m]	3.30E-11[c]	15.4	3.56E-12[c]	74.5
98	9.06E-11[m]	8.36E-11[c]	6.1	3.53E-11[m]	7.5
120	N/A	1.58E-10[c]	3.2	1.37E-10[m]	1.9
150	N/A	3.39E-10[c]	1.5	9.92E-10[m]	0.3

[c]:calculated value based on Arrhenius equation derived from the data at temperature 98, 120 and 150 °C[m]: measured value. t_s is time to saturated the sample with water. $t_{1/2}$ is the time taken to reduce M_n by 50%.

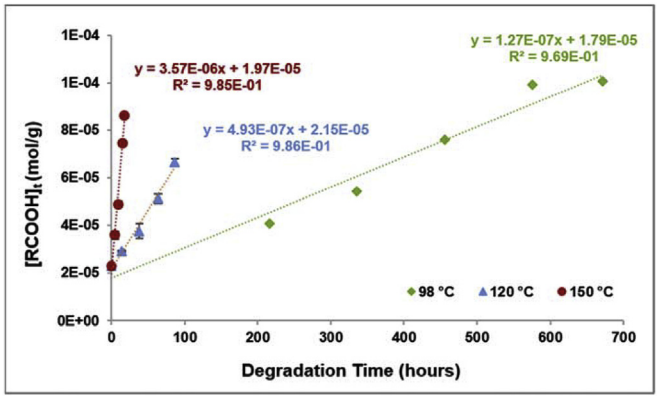

Fig. 2. The plots of $[RCOOH]_t$ vs. degradation time t at 98 °C (green diamond), 120 °C (blue triangle) and 150 °C (red dot). (For interpretation of the references to color in this figure legend, the reader is referred to the Web version of this article.)

Table 2
The rate of properties change at each temperature.

Temperature (°C)	k_c (s^{-1})	k_E (s^{-1})
98	5.56E-08	5.43E-05
120	2.78E-07	3.20E-04
150	1.58E-06	1.91E-03

4.2. Change of crystallinity and storage modulus

The morphology of the PBT-PTMG is best described as hard segment PBT domains dispersed in a soft segment matrix of PTMG, in which some PBT blocks are covalently linked to PTMG [9,16]. The hard PBT crystalline domains function as physical crosslinks. DSC scans reveal some morphology changes of the PBT-PTMG before and after hydrolytic degradation. Fig. 3 shows the DSC scan of the samples aged at 120 °C at varying time intervals. The melting temperature of the original sample, T_{m1}, is 217.2 °C with a small shoulder (T_{m2}) at around 220.4 °C; the crystallization temperature, T_c, on the cooling cycle, is at 172.5 °C (the peak temperature of the exothermic peak). As the degradation time increases, the intensity of T_{m2} increases and the peak moves to 223 °C after almost four days of degradation in water at 120 °C. Meanwhile, T_c gradually increases as the degradation proceeds accordingly as shown in Fig. 3. Thus, the undercooling ΔT ($\Delta T = T_m^0 - T_c$, T_m^0 is the equilibrium melting temperature) decreases for the degraded samples, which indicates easier formation of a crystalline phase in the degraded samples. The rate of the change of T_c is also temperature-dependent and the samples that degraded at higher temperatures showed a faster increase of T_c (Figure S7, Supplementary Materials), which supports the hypothesis that hydrolysis drives the change of morphology.

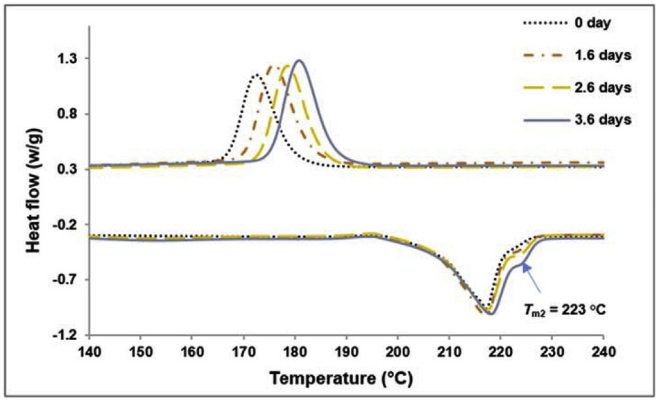

Fig. 3. DSC (1 s t) scans of the dried PBT-PTMG samples before (0 day, black dot) and after degradation for 1.6 days (red dash-dot line), 2.6 days (purple dashed line), and 3.6 days (blue solid line) at 120 °C. (For interpretation of the references to color in this figure legend, the reader is referred to the Web version of this article.)

T_{m2} of the degraded samples increases to be closer to the T_m of pure polybutylene terephthalate (230 °C) [17], which suggest that the newly formed crystalline phases resemble PBT. The percentage of total crystallinity (X_c%) also increases as the degradation proceeds at each temperature. We reason that the change of crystallinity should also follow the pseudo zero order kinetics, Eq. (4), if the change of crystallinity is solely the result of crystallization of the separated PBT blocks originally linked to soft PTMG segments. Fig. 4 indeed shows a reasonable linear correlation of X_c% to the degradation time at 98 °C ($R^2 = 0.98$), 120 °C ($R^2 = 0.98$) and 150 °C ($R^2 = 0.97$). The slopes of the linear plots are the apparent zero order rate constant, k_c (s^{-1}), of the change of X_c % (Equation (4)) at each temperature (Table 2), and the activation energy is calculated to be 84.0 kJ/mol using Arrhenius' Equation with $R^2 = 0.99$ (Figure S8, Supplementary Materials).

$$\frac{dX_c\%}{dt} = k_c \qquad X_{ct}\% = k_{ct} + X_{c0}\% \tag{4}$$

Since water diffusion and hydrolytic degradation take place mostly in the amorphous phase [18] and there is little weight loss at this stage of degradation, the increase of X_c% following the degradation should be the result of hydrolysis induced chemicrystallization [19] of the PBT segments that were originally linked to the PTMG soft segments in the amorphous phase and are 'freed' after the hydrolysis of the ester bonds. These PBT segments have relatively long polymer chains and thus form larger sizes of PBT crystals [20]. Fayolle and Richaud have shown that the X_c% for quenched semi-crystalline polymers is inversely proportional to the square root of molecular weight [19]. In Fig. 5, the linear relationship of X_c% and $M_n^{-1/2}$, for all the experimental samples regardless of their degradation history, suggests that the simple relationship between crystallinity and molecular weight is also correct for hydrolysis induced chemicrystallization for this polymer.

Transmission electron microscopy (TEM) confirms the evolution of the morphology before and after degradation. The samples were stained with phosphotungstic acid (PTA) so the crystalline phase is visible as a light/bright fibrillary region under TEM [9]. Scheme 1 shows the TEM images of the original sample (left) and the dried sample after degradation in water at 150 °C for 15 h (right). Both images present the light fibrillary crystalline lamellar as being 30–35 Å in width that are continuous and interconnected by short lengths of tie molecules (Scheme 1, left). The difference lies in the

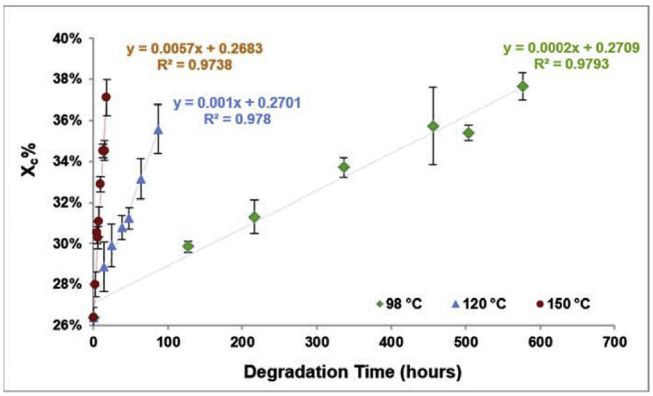

Fig. 4. The plots of X_c% vs degradation time t at 98, 120, and 150 °C.

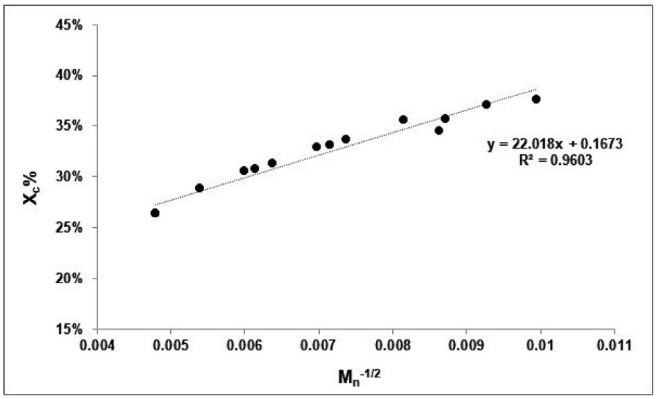

Fig. 5. The linear plot of X_c% vs. $M_n^{-1/2}$ for all the samples degraded at three temperatures.

dark amorphous phase [9]. The amorphous phase of the degraded sample is occupied (Scheme 1, right). Scheme 1 bottom also illustrates the proposed evolution of the morphology of the elastomers before and after degradation.

The morphology change of the samples after degradation affects the mechanical properties of the polymer. We measured the storage modulus E' of the dry samples before and after degradation using a DMA temperature sweep from 25 °C to 160 °C. The degraded samples show overall higher E' than the original samples across the whole temperature range (Figure S9, Supplementary Materials). To further compare the E' of the samples with different degradation history, we recorded the "median plateau modulus" [21] E' at 100 °C for each sample before and after degradation at different temperatures. The E' at 100 °C of the degraded elastomers increases and follows the pseudo zero order kinetics to the degradation time at 98, 120 and 150 °C with R^2 at 0.97, 0.96 and 0.99 respectively (Fig. 6). The slopes of the plots in Fig. 6 are the apparent rate constants, k_E (s^{-1}) of the change of E' at each degradation temperature (Equation (5)). The activation energy is calculated to be 89.2 kJ/mol (Figure S10, Supplementary Materials).

$$\frac{dE'}{dt} = k_E \qquad E'_t = k_{Et} + E'_0 \tag{5}$$

The hydrolysis activation energy, crystallinity change and modulus change are in the narrow range of 84–89 kJ/mol, which strongly suggests that the same mechanism drives their change. Dividing Equation (5) by Equation (4) gives rise to Equation (6), which suggests that the E' should be linearly proportional to X_c % with the slope close to k_E/k_c regardless of the thermal history of the samples. Figure S11 in the supporting materials indeed shows the approximate linear plot of E' vs X_c% ($R^2 = 0.91$) for all the samples before and after degradation. The *slope* of the E' vs X_c% plot is 1069, close to the slope of k_E vs k_c plot (Figure S11). This correlation strongly indicates that the increase of crystallinity drives the increase of the storage modulus and the decrease of M_n has little impact on the storage modulus.

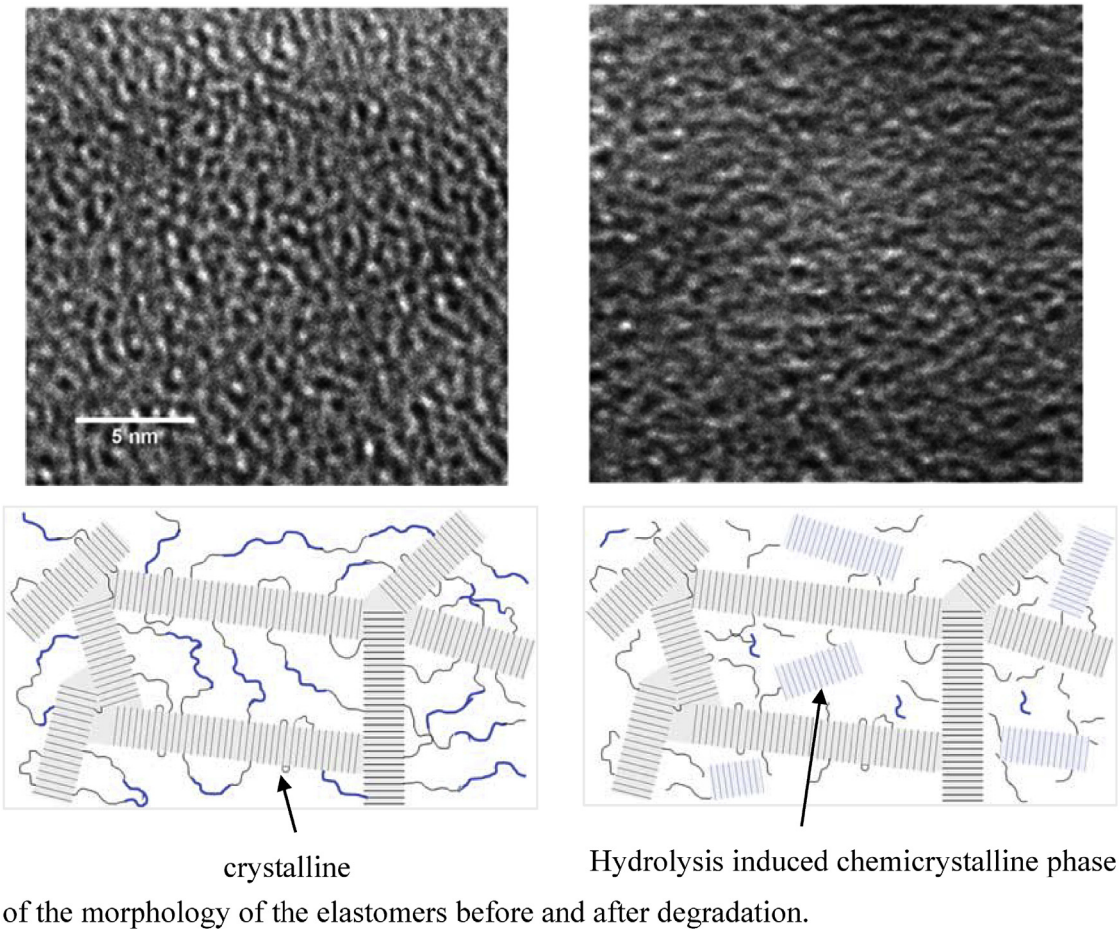

Scheme 1. Top: TEM images of the dry elastomer samples before (left) and after degradation at 150 °C for 15 h (right). Bottom: illustration of the phases of the TPE before (left) and after degradation (right).

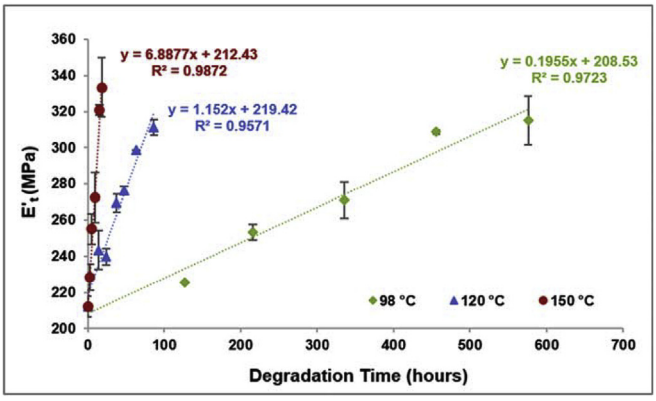

Fig. 6. The change of E' vs degradation time t at 98, 120 and 150 °C.

$$\frac{dE'}{dX_c\%} = \frac{k_E}{k_c}\ ,\ E' = \frac{k_E}{k_c}X_c\% + A' \tag{6}$$

4.3. Tensile strength

The large strain mechanical properties of the PBT-PTMG samples (1.5 mm in thickness) under uniaxial tension demonstrate a transition from ductile to brittle behavior upon hydrolytic degradation. The neat material ('Ref') fails at around 600% engineering strain and 60 MPa engineering stress (Fig. 7). The stress-strain curves are conventionally described in three parts: the pseudo elastic region below the yield stress, the "draw" region, where the neck propagates and the hard phase crystallites are aligned, and the strengthening region, similar to an elastomeric curve [8].

After three days of exposure to water at 120 °C and the subsequent drying, the samples fail at 5% strain, below the yield, and 22 MPa. The stress-strain curves of the degraded and dried samples fit on a master-curve, with a slight increase in yield stress with increasing degradation time (Fig. 7). Pictures in Fig. 7, right, show the samples after failure. They illustrate that the samples degraded for 1.6 days exhibit a necking region, while the 3-day sample displays a brittle failure. Both the ductile-to-brittle transition and the increase in yield stress are consistent with the crystallinity increase that accompanies the disruption of the soft segments described above. The change in the stress-strain curve is a reflection of the decrease of the number average molecular weight (M_n) and increase of the crystallinity (increase of the tie molecules) [22] after the hydrolytic degradation. After the first two days of degradation at 120 °C, the M_n decreased from around 44 kg/mol to around 17 kg/mol (Figure S5, Supplementary Materials) along with the increase of crystallinity from around 26%–33%, which results in the increase of the yield stress and decrease of the ultimate tensile stress and strain.

Figs. 8 and 9 synthesize the tensile results for all the samples tested right after water exposure (wet) and dried for one week (dry). After around one day in water at 120 °C, the samples fail at an average ultimate stress below their yield stress. In other words, they do not show any hardening behavior, further proving the disruption of the soft, elastomeric phase. In this region, the strength of the material is equal to the yield stress, which is rather constant (wet) or slightly increasing (dry) with increasing degradation time. The water acts as a plasticizer in the wet state, counteracting the increased

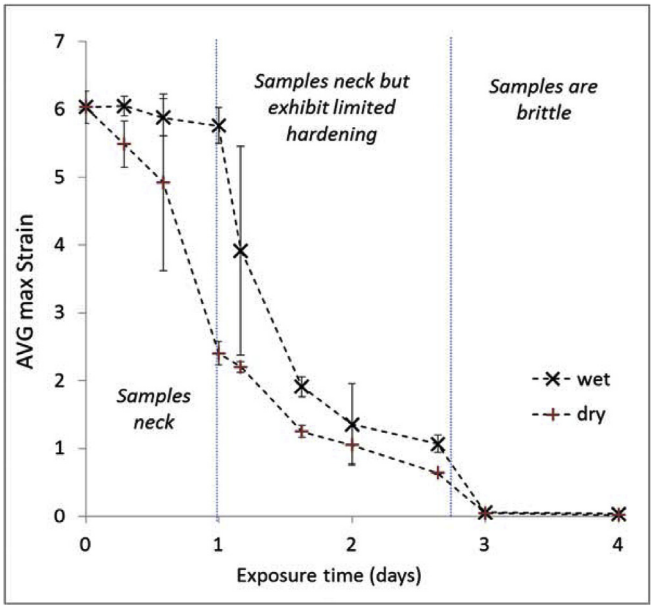

Fig. 8. Uniaxial tensile test results for all samples – Evolution of the ultimate strain vs. time of water exposure at 120 °C, for wet and dry samples.

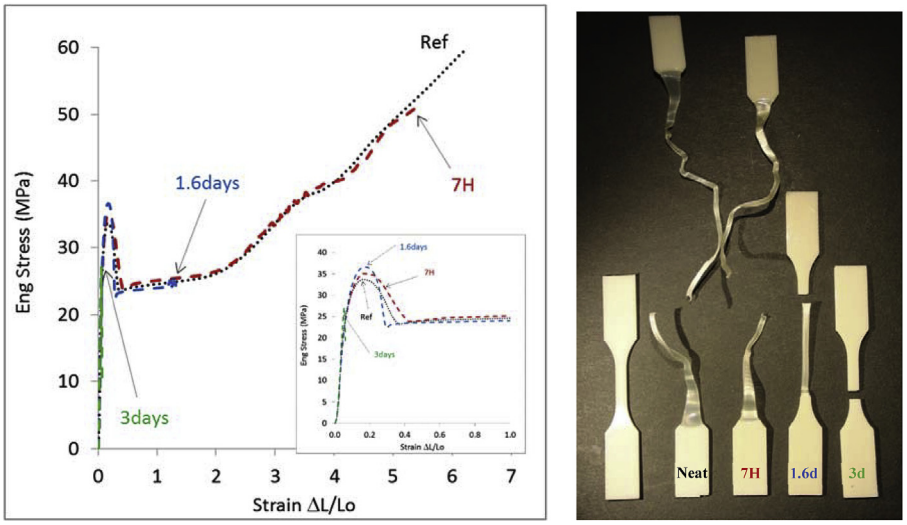

Fig. 7. Uniaxial tensile test results – Samples tested after hydrolytic degradation at 120 °C for 7 hrs, 1.6 days and 3 days, and subsequent drying. Right: Pictures of the post-mortem samples. Inset: Zoom.

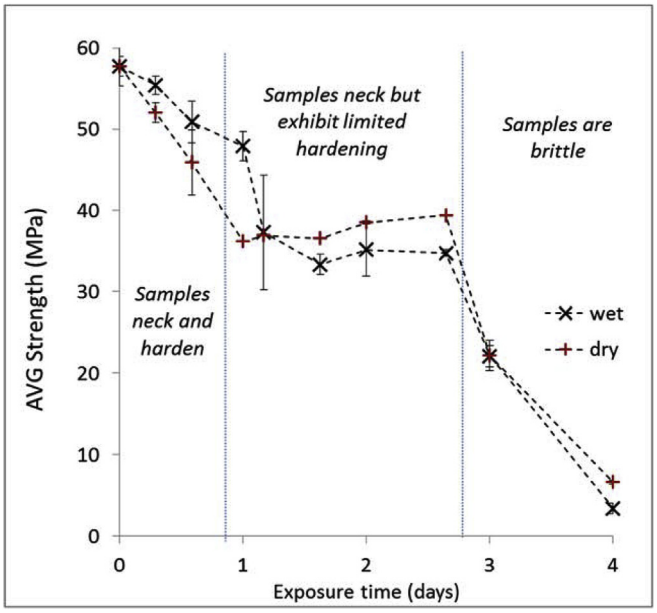

Fig. 9. Uniaxial tensile test results for all samples – Evolution of the strength vs. time of water exposure at 120 °C, for wet and dry samples.

crystallinity related to hydrolytic degradation. Between 2.6 and 3 days, the samples become brittle, i.e. they fail before yielding. Interestingly, the half time (time to degrade half of the ester bonds) is 2.4 days at 120 °C, which is close to the time it takes to make the samples brittle (between 2.6 and 3 days with M_n below 20 kg/mol). In summary, the evolution of the tensile stress and strain during the degradation is the result of the changes at the molecular level.

5. Conclusion

We studied the hydrolytic degradation of the PBT-PTMG at elevated temperatures from both a mechanical and chemical perspective, and have determined the Fickian diffusion coefficient, the rate of hydrolysis, the change in crystallinity and the storage modulus with respect to varying temperature and time. Our results indicate that the chemical degradation via hydrolysis follows pseudo zero order kinetics, and the kinetics of hydrolysis correlates with the rates of change of crystallinity and modulus. In fact, chain scissions due to hydrolysis lead to the reduction of the molecular weight and decrease of tensile strength and strain; rearrangement of molecular fragments increase crystallinity (chemicrystallization); rise of crystallinity increases the storage modulus regardless of the samples' thermal history. Applying Arrhenius' empirical relationship to the determined rates gives rise to a temperature-dependent model. The model allows for a good approximation of the behavior of the mechanical properties at temperatures outside of the experimental range based on the activation energies. The rather large temperature range (~50 °C) used to determine the temperature dependence of each property makes the model more robust; however, extrapolation should be done with caution, especially when approaching the glass transition temperature (25 °C) and the melting point (218 °C).

Appendix

Measurement of water diffusion coefficient are made on dried rectangular prism samples of the PBT-PTMG measuring approximately 3 × 4 × 22 mm. Samples were subjected to isothermal water absorption experiments at 38, 70 and 98 °C. The mass and volume of each original sample were measured using a Sartorius CPA1245 analytical balance (Data Weighing Systems). The width and thickness were measured using a Mitutoyo digital caliper. Three samples were placed in glass vials containing 10 ml of deionized (DI) water. The samples in the sealed vials were placed in an oven at the desired temperature and the mass of the wet samples was measured periodically after removing the surface water using Kimwipes. The sample was considered saturated with water once the wet weight reached a plateau.

6.1. Fickian diffusion coefficient

Determining the Fickian Diffusion coefficient allows for the quantification of water absorption and enables a comparison of the kinetics of water absorption with that of hydrolysis. We used the 1D Fickian diffusion model (Equation (A1)) to derive the Diffusion coefficient (D_x) at each temperature [23]. In Equation (A1), m_t is the mass of the wet sample at time t, m_i is the mass of the original dry sample, m_{max} is mass of the wet sample at water saturation and $H_2O\%$ (max) is percentage of water absorption at saturation.

Fickian 1D Diffusion Infinite Plate Geometry Equation

$$\frac{m_t - m_i}{m_{max} - m_i} = 1 - \frac{8}{\pi^2}\sum_{j=0}^{\infty}(2j+1)^{-2} \times \exp\left[-\frac{(2j+1)^2\pi^2 D_x t}{a^2}\right] = \frac{H2O\%\,(t)}{H2O\%\,(max)} \quad \text{(A1)}$$

$a < b < c$ (*dimensions of a rectanguloid*), $D_x \cong f^{-2}Deff$

Equation (A1) is developed for an infinite plate that has one-dimensional diffusion. Since the geometry of the experimental samples deviates from an infinite plate, an edge correction factor ($f \approx 1.5$ when a = 3 mm, b = 4 mm and c = 22 mm for our samples) [23] is applied to get the more accurate 1D diffusion coefficient (D_x) for the experimental samples. An unconstrained optimization algorithm in MATLAB called "fminsearch", which applies the least square function to minimize the residual distance between a predicted/estimated D_x and the actual (experimental) D_x, was used to derive the optimal D_x from the experimental data collected at each temperature.

6.2. Diffusion coefficient of water absorption

The mass of each sample increases as the sample absorbs water over time, though the dimension change is inconspicuous (within the experimental error) (Supplementary Materials, Figure S2). Figure A1 shows the mass% increase over time at 38, 70 and 98 °C. Within the time frame of the water absorption experiments, the leaching of chemicals to water is minimum as there is little weight change after the absorbed water is removed by vacuum. Applying an unconstrained optimization algorithm "fminsearch" in MATLAB to the average $H_2O\%$ results in the optimal 1D diffusion coefficient D_x at each temperature (Figure A2 and Table 1). The activation energy E_a for D_x is calculated to be 35.2 kJ/mol ($R^2 = 0.99$, Figure A3).

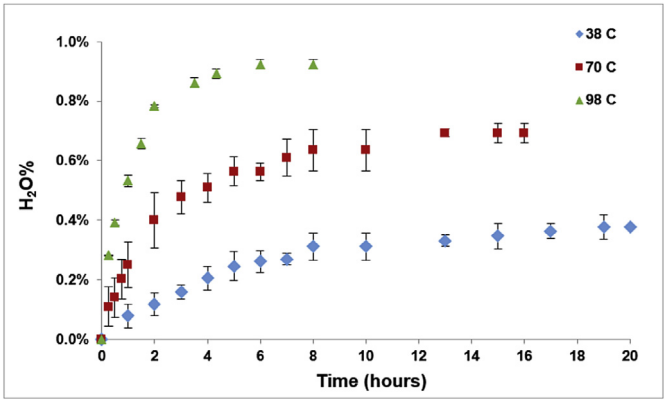

Fig. A1. Average H_2O% absorbed into the samples at isothermal 38, 70 and 98 °C in water.

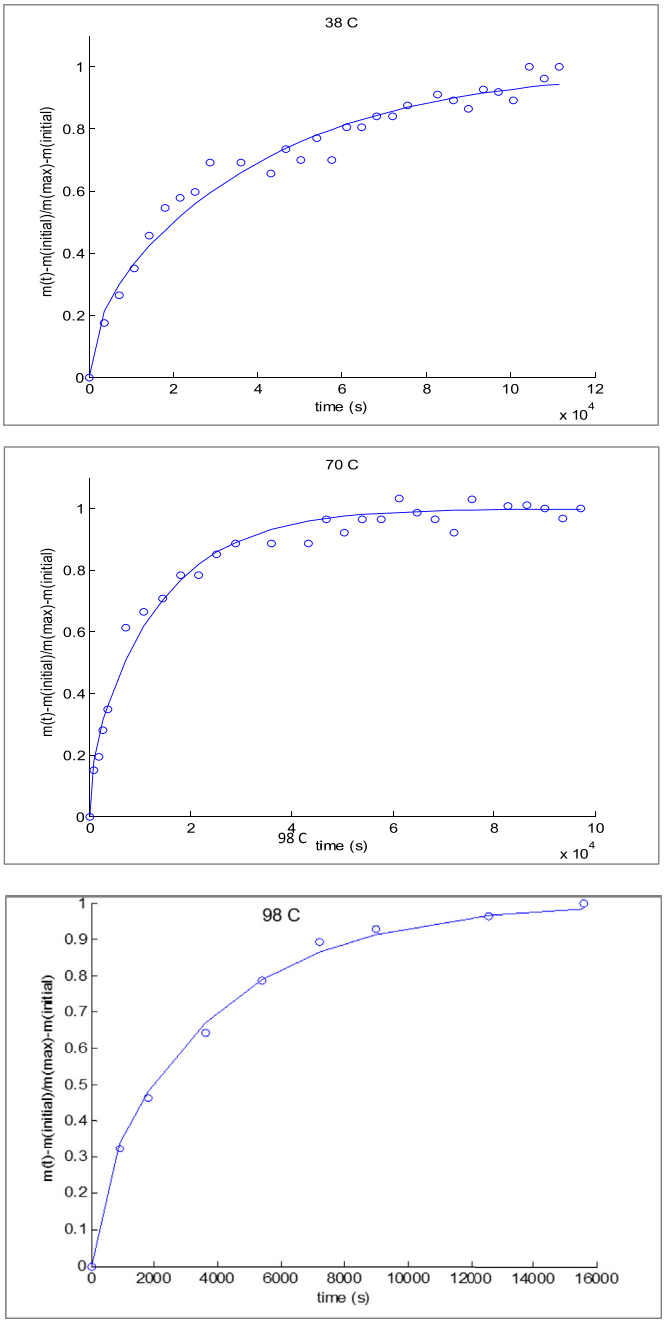

Fig. A2. The 'fminsearch' fitting of water absorption data using Equation (A1). Top: 38 °C, middle: 70 °C, and bottom: 98 °C.

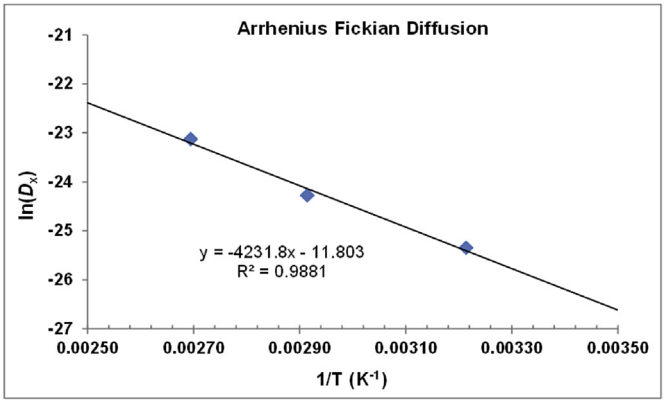

Fig. A3. Arrhenius plots of coefficient D_x of isothermal water diffusion at 38, 70 and 98 °C. E_a is 35.2 kJ/mol.

Appendix A. Supplementary data

Supplementary data related to this article can be found at https://doi.org/10.1016/j.polymdegradstab.2018.07.002.

References

[1] J.F. Patrick, et al., Polymers with autonomous life-cycle control, Nature 540 (2016) 363.
[2] S.-W. Hwang, et al., A physically transient form of silicon electronics, Science 337 (2012) 1640–1644.
[3] M. Qu, et al., Zinc oxide nanoparticles catalyze rapid hydrolysis of poly(lactic acid) at low temperatures, J. Appl. Polym. Sci. 131 (11) (2014) 5–12.
[4] A.-D.N. Celestine, S.S. Zhu, Effect of temperature and moisture on the mechanical properties of fiber reinforced nylon 6 composites. Challenges in mechanics of time dependent materials, in: Volume 2 Proceedings of the 2016 Annual Conference on Experimental and Applied Mechanics, (Chapter 14), 2016.
[5] X. Dai, Z. Qiu, Crystallization kinetics, morphology, and hydrolytic degradation of novel biobased poly(butylene succinate-co-decamethylene succinate) copolyesters, Polym. Degrad. Stabil. 137 (2017) 197–204.
[6] J.G. Drobny, Handbook of Thermoplastic Elastomers Introduction. William Andrew Publishing/Plastics Design Library, 2007.
[7] Odian, G., Principles of Polymerization. third ed.: p. 148–149.
[8] H. Schmalz, et al., Morphology, surface structure, and elastic properties of PBT-based copolyesters with PEO-b-PEB-b-PEO triblock copolymer soft segments, Macromolecules 35 (2002) 5491–5499.
[9] R.J. Cella, Morphology of segmented polyester thermoplastic elastomers, J. Polym. Sci.: Symposium 42 (1973) 727–740.
[10] J.G. Drobny, Handbook of Thermoplastic Elastomers 11. Thermoplastic Polyether Ester Elastomers, 2007.
[11] Q. Zhou, M. Xanthos, Nanoclay and crystallinity effects on the hydrolytic degradation of polylactides, Polym. Degrad. Stabil. 93 (2008) 1450–1459.
[12] C.G. Pitt, Z.W. Gu, Modification of the rates of chain cleavage of polyaprolactone and related polyesters in the solid state, J. Contr. Release 4 (1987) 283–292.
[13] W. Zaiqing, S. deyan, Z. hengqi, The Rheo-optical FTIR study of Polyesterpolyether segmented copolymer Chinese, J. Polym. Sci. 6 (4) (1988) 325–331.
[14] S. Radhakrishna, D.R. Saini, M.V. Kuber, Effect of morphology on the dielectric properties of a segmented copolymer, Eur. Polym. J. 27 (3) (1991) 291–297.
[15] H.A. Pohl, Determination of carboxyl end groups in a polyester, polyethylene terephthalate, Anal. Chem. 1614 (1954) 1614–1616.
[16] R.W. Seymour, J.R. Overton, L.S. Corley, Morphological characterization of polyester-based elastoplastics, Macromolecules 8 (3) (1975) 331–335.
[17] C.-S. Park, et al., Crystallinity morphology and dynamic mechanical characteristics of PBT polymer and glass fiber-reinforced composites, J. Appl. Polym. Sci. 86 (2002) 478–488.
[18] M. Horstmann, M. Urbani, W.S. Veeman, NMR study of water bound to soft segments in thermoplastic elastomers, Macromol. Symp. 205 (2004) 129–142.
[19] B. Fayolle, et al., Review: degradation-induced embrittlement in semi-crystalline polymers having their amorphous phase in rubbery state, J. Mater. Sci. 43 (2008) 6999–7012.
[20] W. Gabrie1lse, M. Soliman, K. Dijkstra, Microstructure and phase behavior of block copoly(ether ester) thermoplastic elastomers, Macromolecules 34 (2001) 1685–1693.
[21] G.K. Hoeschele, Segmented polyether ester copolymers-a new generation of high performance thermoplastic elastomers, Polym. Eng. Sci. 14 (12) (1974) 848–852.
[22] L.E. Nielsen, Mechanical Properties of Polymers and Composites, vol. 2, 1974, p. 275.
[23] M.J. Starink, L.M.P. Starink, A.R. Chambers, Moisture uptake in monolithic and composite materials: edge correction for rectanguloid samples, J. Mater. Sci. 37 (2002) 287–294.